ACS APPLIED POLYMER MATERIALS

pubs.acs.org/acsapm Article

Influence of Inorganic Glass Ceramic Particles on Ion States and Ion Transport in Composite Single-Ion Conducting Gel Polymer Electrolytes with Varying Chain Chemistry

Emily S. Doyle, Hunter O. Ford, David N. Webster, Peter J. Giannini, Meghanne E. Tighe, Robert Bartsch, Graham F. Peaslee, and Jennifer L. Schaefer*

Cite This: ACS Appl. Polym. Mater. 2022, 4, 1095−1109 Read Online

ACCESS | Metrics & More | Article Recommendations | Supporting Information

ABSTRACT: A major goal of next-generation battery development is the engineering of nonflammable solid-state electrolytes with high enough ionic conductivity to compete with traditional liquid electrolytes. Composite polymer electrolytes (CPEs), which combine inorganic fillers or electrolytes with a polymer matrix, are seen as a strategy to boost the ionic conductivity of flexible polymer electrolytes while overcoming the brittle aspect of inorganic electrolytes. In this work, we examine the impact of polymer backbone chemistry on Li^+ ion conduction within crosslinked single-ion conducting gel polymer electrolytes (SIPEs) that contain a lithium ion-conducting glass ceramic electrolyte (LICGC). Certain SIPE compositions based on poly(tetrahydrofuran) diacrylate (PTHFDA) crosslinking macromonomers exhibit a significant increase in conductivity with the inclusion of LICGC, a result unexpected from prior literature. With the use of Raman spectroscopy, small angle X-ray scattering, and particle-induced gamma-emission spectroscopy (PIGE), it is proposed that the enhanced conductivity comes from the formation of percolated LICGC particles sheathed in an ion-rich domain. This region develops in the pre-polymer solution due to interactions between the LICGC particle surface and the ionic comonomer, much like the formation of space-charge regions in soggy-sand liquid electrolytes, and persists post-polymerization to yield a CPE of enhanced conductivity. The particle−ionic monomer interactions are modulated by the crosslinking macromonomer polarity, polymer casting solvent, and particle surface area. While there is ample room for continued optimization, the best SIPEs in this study are capable of Li metal dissolution/deposition, and they reach Li^+ conductivities greater than 2×10^{-4} S/cm at 25 °C, surpassing the practical use threshold.

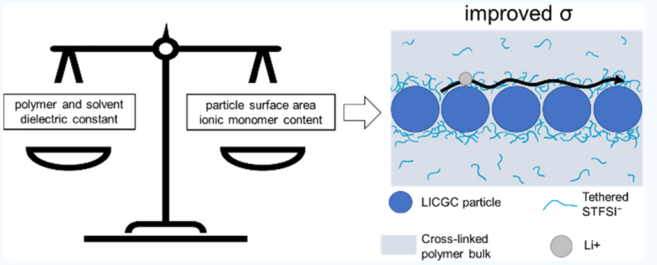

KEYWORDS: *batteries, composite polymer electrolyte, soggy-sand, ion transport, single-ion conductor*

INTRODUCTION

A surge in polymer electrolyte (PE) research aims to minimize the safety concerns associated with the flammability and electrochemical instability of current liquid electrolyte systems.[1−6] Despite their advantages in these areas, PEs are not currently viable materials for room temperature battery operation because of their low lithium-ion conductivities on the order of 10^{-8} to 10^{-5} S/cm, while liquid electrolytes exhibit conductivities on the order of 10^{-2} S/cm.[2,7,8] Another challenge impacting both liquid and polymer electrolytes is the passivation of the electrodes by electrolyte salts.[9]

Single-ion conducting polymer electrolytes (SIPEs) contain only anions covalently bound to the polymer chains to prevent long-range anion motion.[10] SIPEs demonstrate lithium transference numbers near unity, which mitigates the development of anion concentration gradients across the cell and the subsequent decomposition of concentrated salts on the electrodes, granting cells faster charging/discharging, higher cycling efficiency, and longer life due to enhanced ion transport.[10,11] The most substantial technical challenge for SIPEs is low ionic conductivity. Several papers in recent years discuss macromolecular chemistry and design strategies aimed at improving the ionic conductivity of SIPEs.[12−16] In short, the use of bound anions with increased charge delocalization and miscibility with the organic matrix that reduces formation of dense ionic aggregates and enhances lithium cation dissociation tends to result in improved ionic conductivity for both the dry polymer and gel cases.[13,17−19] Typical solvent-gelled SIPE conductivity lies on the order of 10^{-4} S/cm.[20] Top performing gel SIPEs with nanostructured polymer matrices exhibit ionic

Received: November 4, 2021
Accepted: January 6, 2022
Published: January 21, 2022

https://doi.org/10.1021/acsapm.1c01535
ACS Appl. Polym. Mater. 2022, 4, 1095−1109

conductivities on the order of 10^{-3} S/cm when containing organic carbonate solvents.[21,22]

Composite polymer electrolytes (CPEs) have been studied to address the poor conductivity of pure PEs. PE advantages include ease of fabrication, enhanced interfacial contact, higher electrochemical stability against electrodes, and low density.[4,23] Inorganic electrolytes have unity transference numbers like SIPEs, and some have excellent conductivities on the order of 10^{-4} to 10^{-2} S/cm, but they are often brittle and have high processing costs and low electrochemical stability against electrodes, with notably low stability against lithium metal.[1,7,24] Many pure inorganic electrolytes require thin interfacial polymer adhesives to increase electrode/electrolyte contact and minimize electrolyte degradation. Therefore, development of an inorganic-in-PE, as presented in this work, would simplify the cell design by adopting the strengths of the polymer at the electrode interfaces and the bulk transport and mechanical properties of the inorganic component.[25] It is believed that the proper combination of the inorganic and polymer components could yield a CPE with high conductivity, processability, mechanical properties, and electrochemical performance.[9,23,26] A remaining question is how the inclusion of inorganics within CPEs and interactions between the inorganics and polymer components alter ion conduction mechanisms, the answers to which will lead to improved design metrics for high-performance CPEs.

Current studies of CPEs report different lithium transport pathways, and the direct impact of the inorganic inclusions on ion transport is unclear. A key aspect of this research revolves around elucidating the effect of inorganic inclusions on ion coordination behavior. Judez and colleagues approached this problem by observing the transference number of dual-ion conducting PEs with and without an inorganic additive, specifically a NASICON-type $Li_{1.5}Al_3Ti_{1.7}Si_{.2}P_{2.8}O_{12}$ (LATP) active glass ceramic from Ohara Corporation called lithium ion conducting glass ceramic (LICGC).[26,27] The group found that the addition of the inorganic particles increased the transference number from that of the pure PE and concluded that the inorganic media was able to coordinate with anions, suppress the anion motion, and facilitate the dissociation of the lithium cation for increased transport.

Merrill and colleagues supported this conclusion with their work on CPEs in which they compared conductivity and anionic coordination states of composite poly(ethylene oxide) PEs with varying loadings of LICGC.[11] They found that high conductivity and high coordination of the anion in composite samples were directly correlated, leading to the conclusion that the inorganic coordinates with the anion to displace the lithium cations for faster conduction.

In another work, Chen and colleagues used neutron scattering to interrogate the structure of the composite matrix.[9] This work showed that the segmental dynamics of the polymer phase are inhibited by LICGC inclusion. The results also revealed that the lithium cations are attracted to the inorganic particle surface, and the cations can continue to complex with ether units on the polymer backbones while near the particle. Ion transport along the polymer−inorganic component interface is often related to Lewis acid−base interactions that support fast lithium salt dissociation.[28,29] Inorganics with surfaces that solvate the salts may increase the concentration of lithium cations available for charge transport and potentially decouple the ion transport from segmental motion of the polymer matrix.

Prior studies have demonstrated that inorganic inclusions alter the complexation of charged species, which may impact the bulk conductivity. Yet few studies have investigated the impacts of inorganic additives on single-ion conducting polymer systems. Here, we investigate lithium conductivity and coordination of anions in crosslinked, single-ion conducting composite gel PEs with crosslinking macromonomers of varying chemistry. The effects of crosslinker chemistry are investigated in composites containing LICGC inorganic particles to characterize the dependence of ion conductivity on polymer backbone polarity and solvent type.

Our previous work with SIPEs demonstrates that gel SIPE conductivity is highly dependent on the polymer crosslinker chemistry, which will be probed further in this work to understand how crosslinker chemistry modulates the influence of the inorganic particles on ion transport.[11] Given the prior literature, the inclusion of the Li-ion conducting inorganic particles in solvent-gelled SIPEs leads to five hypothetical modes of lithium-ion transport: via vehicular transport of solvated cations, polymer chain segmental motion, the bulk of the particles with ion hopping between inorganic islands, ion hopping between anionic sites, and particle surface-mediated transport at the polymer/inorganic interphase.[4,7,19,30] Prior studies have shown conclusively with ^{7}Li and ^{6}Li NMR that Li^+ conduction through the volume of inorganic particles has not been observed in CPEs with low inorganic loading, a result attributed to high interfacial resistance to ion transport across the inorganic-polymer interface. Therefore, the primary modes of ion transport in our amorphous gel polymer system are expected to exclude transport through the bulk of the Li-ion conducting LICGC particles.[1,7,27] Nonetheless, inclusion of inorganics in the particulate form is anticipated to be a relevant approach with lower cost than sintered, continuous inorganics. Additionally, the polarity of the crosslinker, defined by the dielectric constant, dictates the miscibility of the components in the composite SIPE. A crosslinker with a high dielectric constant will mix well with the charged anionic monomers and contributes to the dissociation of lithium salts.[23,25] The miscibility of the crosslinker and the anions is expected to alter the dominant transport mechanism within the electrolyte, and this study of transport behaviors with crosslinkers of varying chemistries is imperative to developing a high-performing composite SIPE.

Here, we find that the chemistry of the crosslinking macromonomer, specifically the crosslinking macromonomer polarity, can dictate a host of CPE characteristics that influence performance. Such characteristics include the gelling capacity of the network, the polymer−ion interaction strength, the particle−-ion interaction strength, and formation of long-range ion domains. The crosslinking macromonomer polarity appears to alter the distribution of ionic substituents within the polymer, changing the strength of inorganic particle−ionic monomer interactions. Coordination dynamics are drawn from Raman spectroscopy of the CPEs, where the coordinated and free anion bands are distinct, and spectra can be analyzed to deliver the population densities of the anion in each state.[11,19,31] This degree of ionic association influences the ion transport, and it is found that the LICGC creates new coordination environments that facilitate ion transport. The polymer order is studied by small angle X-ray scattering (SAXS) to develop an understanding of the ion agglomeration and spacing within the material, where it is found that, at least on the scale of ion−ion correlations, inclusion of the LICGC

https://doi.org/10.1021/acsapm.1c01535
ACS Appl. Polym. Mater. 2022, 4, 1095−1109

does not alter the short-range ionic structure. An ion beam analysis technique known as particle-induced gamma-ray emission (PIGE) spectroscopy is leveraged to quantify the amount of mobile lithium in the composite material, whereby it is conclusively determined that cation transport through the LICGC particles is negligible.

Taken in whole, the results of this work show that a certain degree of inorganic−ionic monomer interaction is beneficial for creating highly conductive domains that persist in the final crosslinked CPE. Further, the inorganic−ionic monomer interaction strength is tunable, where altering the chemistry of the prepolymer solution (by varying crosslinking macromonomer chemistry, casting solvent, or particle surface area) influences the degree of inorganic−ionic monomer interaction. The materials are akin to so-called "soggy-sand" electrolytes, where interactions between the inorganic particles and ionic monomer in the pre-polymer solution can produce a percolated space-charge region near the particle surface that produces fast Li^+ conduction at the particle/polymer interphase.[32,33] Unlike liquid soggy-sand electrolytes, the percolated ion transport domain is permanently locked into place when the pre-polymer solution is crosslinked, yielding a composite single-ion conducting polymer electrolyte with stable regions of enhanced ion transport. Proper formulation of the CPEs can produce an electrolyte capable of Li metal dissolution and deposition, with significantly elevated conductivity compared to the inorganic-free PE electrolyte, with the best gel electrolyte displaying a conductivity of over 2×10^{-4} S/cm at 25 °C. Being a single-ion conductor, this composite gel electrolyte meets the conductivity threshold requirement for practical use. These findings inform the development of high-performance CPEs, outlining the parameter space that influences the formation of beneficial ion transport domains and providing a basis for future optimization.

EXPERIMENTAL SECTION

Poly(Ethylene Glycol) Diacrylate (PEGDA) and Poly(Tetrahydrofuran) Diacrylate (PTHFDA)-Based Composite Gel Polymer Electrolyte Film Fabrication. First, 0.06 g of ionic monomer 4-styrenesulfonyl (trifluoromethyl-sulfonyl)imide potassium salt (KSTFSI) was dissolved in 1.2 g of tetraglyme (TEG) (>99%, Sigma) with low heating. KSTFSI was synthesized as described in our previous work and in the literature.[19,34,35] Then, 0.39 g of the PTHFDA ($\overline{M_n}$ about 700 g/mol) or PEGDA ($\overline{M_n}$ 700 g/mol; Sigma Aldrich) was added and allowed to dissolve. PTHFDA was prepared from poly(tetrahydrofuran) ($\overline{M_n}$ 650 g/mol; Sigma Aldrich) as outlined in our previous work.[19] For the composite polymers, the LICGC particles (1 μm, Ohara) were then added at 30 wt %. This wt % was chosen because of its good performance in the literature in similar PEGDA-based ionomers.[19] The mixture was then stirred for 20 min with constant bubbling of N_2 to expel oxygen, which may hinder the polymerization reaction, from the monomer solution. After mixing, 0.018 g (4 wt % with respect to the monomer mass) of the initiator 2,2-azobisisobutyronitrile (AIBN, 98%, Sigma Aldrich) was dissolved in the solution. The AIBN was recrystallized from methanol before use. Stirring with N_2 is continued for 10 more minutes. The inclusion of the inorganic particles results in a uniform suspension of moderate viscosity that may be considered of the so-called "soggy-sand" type solution.[33] This solution was then prepared for polymerization by sandwiching it between two glass slides with uniform thickness enforced by 100 μm glass coverslip slides and placed in an oven at 75 °C for 3 h. After the polymerization time, the polymers were removed from the oven and rinsed with methanol to remove the excess monomer solution. The PEGDA-based polymers were then submerged in a 0.5 M lithium chloride (LiCl) in water solution to exchange the potassium cations from the KSTFSI monomer with lithium cations. PTHFDA-based polymers were submerged in 0.5 M LiCl in methanol instead of water for ion exchange. The solution was replaced once daily for 2 days. Then the polymer was rinsed with pure water or methanol, as appropriate, replaced once daily for 2 days to remove excess salt from the material. The polymers were then left out to dry in open air before loading into the glovebox to be dried under dynamic vacuum at 80 °C for 16 h.

Poly(Dimethyl Siloxane) Diacrylate (PDMSDA)-Based Composite Gel Polymer Electrolyte Film Fabrication. Synthesis of the PDMSDA-based ionomer follows a similar method. First, 0.06 g of KSTFSI was dissolved in 0.6 g of TEG with low heating. Then, 0.39 g of PDMSDA (methacryloxypropyl terminated poly(dimethyl siloxane), Gelest Inc., $\overline{M_n}$ 900−1200 g/mol) was dissolved. In the desired samples, LICGC was added at 30 wt %. This solution was stirred while bubbling through N_2 for 20 min. Then, 4 wt % of AIBN initiator was added, and 10 more minutes of stirring while bubbling N_2 followed. Then, 10 mL of dichloromethane (DCM) (>99.5%, Sigma Aldrich) were bubbled with N_2 for 2 min, and 0.6 g of this solvent was added to the monomer mixture. The addition of the DCM causes the solution to become a single phase, and in solutions containing inorganic particles, the solution is a uniform moderate viscosity suspension. This solution was transferred to a Teflon-lined stainless-steel autoclave in N_2. This autoclave was sealed to prevent DCM evaporation. The autoclave was put in the oven at 75 °C for 3 h. The ion exchange, washing, and final drying steps for the PDMSDA-based polymer were the same as the procedure for the PTHFDA-based polymer.

Ball-Milling of LICGC Particles. LICGC particles were wet ball-milled in TEG solvent. A suspension of 1 g of LICGC and 4.5 g of TEG was added into a nylon jar with four 11.5 mm zirconia milling balls and milled at 1200 rpm for 12 h in a high-speed 3D ball mill (MTI corp.). The milled particles formed a uniform suspension, which was used directly in film fabrication. A small portion of the suspension was dried and studied with scanning electron microscopy for particle size estimation.

Scanning Electron Microscopy (SEM) of LICGC Particles. LICGC particles, pristine or milled, were pressed into conductive carbon tape on top of an SEM sample stub. Images were collected with a beam current of 0.1 nA and voltage of 15 kV on a Magellan 400 FESEM.

Conductivity Measurements. Conductivity measurements were performed on a Broadband Dielectric Spectrometer (Novocontrol, Montabaur, Germany). The fully swelled gel polymer samples were punched into 0.5-inch diameter circles, sandwiched between two polished brass electrodes and then placed in an air-tight sample cell for testing. Frequency-dependent dielectric data was collected over a temperature range of −5 to 85 °C. The DC conductivity was calculated from the plateau of the real conductivity (sigma′) versus frequency curve using a Python script. An example of the raw data is given in the Supporting Information.

Swelling Measurements. Polymer samples were swelled in the propylene carbonate (PC, anhydrous 99.7%, Sigma) solvent, and the degree of swelling by mass and volume was measured. The films were punched in 1/8-inch diameter circles, and the diameter, thickness, and mass of the dry samples were recorded. The samples were swelled overnight in 500 μL of solvent. The weight and dimensions of the swelled samples were then taken, and the percent change in weight and volume were calculated for each sample. This procedure was completed at least three times or until the standard deviation in measurements was less than 15% for each sample type.

Raman Spectroscopy. The samples were analyzed on an NRS-5000 micro-Raman spectrometer from Jasco with an irradiation wavelength of 532 nm. The samples were sandwiched between two borosilicate glass microscope slides. The edges of the slides were sealed to minimize the amount of moisture accessible to the sample. The device was set to the following settings: 20× magnification, 25×1000 μm slit dimension, 4000 μm aperture, 0.5 cm^{-1} resolution, L1200/B500 nm grating, and BS 30:70. All the samples were exposed to the laser for 30 s for 6 accumulations except the PTHFDA sample,

https://doi.org/10.1021/acsapm.1c01535
ACS Appl. Polym. Mater. 2022, 4, 1095−1109

which was analyzed for 20 s and 9 accumulations. This sample was the most transparent and it quickly saturated the detector. The samples produced a severe level of fluorescence, so the device was set to automatically subtract fluorescence from the spectra.

After the set accumulation time, the spectra were monitored for peak formations in the range of 725−760 cm^{-1}. In this range, the fully dissociated and fully associated peaks were expected to appear at 730 and 748 cm^{-1}, respectively.[31,36] The spectra were then processed with a Gaussian fitting program. This program deconvoluted the raw spectra to fit the data with Gaussian functions. At this step, the number of peaks fitted to the data was determined manually based on the number of visible peaks and shoulders in the spectra.

The overall state of association for a material was quantified on a weighted scale from 0 to 1 by assigning each wavenumber from the lowest to highest state a linearly imposed weight from 0 to 1 and multiplying the interpolated weight of each wavenumber in a given sample by that peak's area. The summation of these values over a given sample's spectrum produces a value for the material's overall state of anion association.

Small- and Wide-Angle X-ray Scattering (SAXS/WAXS). Within an Ar glovebox, composite and inorganic-free PE films were cut into thin strips and loaded into 1.5 mm diameter glass capillaries, which were then filled with solvent as appropriate and sealed with wax. X-ray scattering measurements were conducted at the Argonne Advanced Photon Source, at synchrotron beamline 12-ID-B. This beamline is operated by the Argonne National Laboratory Chemical and Materials Science group. The beamline was calibrated with a silver behenate standard and operated at a beam energy of 13.3 keV (0.9322 Å) at a sample distance of 2.01 m. Spectra were background-subtracted to remove the contribution of solvent and capillary. In some instances, overscattering caused by the presence of the LICGC was subtracted out by using the spectra of a PEGDA homopolymer with LICGC, thereby recovering underlying polymer scattering.

Li Isotope-Exchange Sample Preparation and Measurement by PIGE. Standards of varying wt % LICGC within PTHFDA polymer (0, 5, 10, and 25) are prepared in the same manner as the PTHFDA-x-LiSTFSI composite polymers, where the obtained polymer is rinsed free of unreacted material and dried directly in the vacuum oven. The sample of PTHFDA-x-LiSTFSI-LICGC to be exchanged to ^{6}Li was cut into a 5/8″ diameter punch and fully swelled in PC. The same sized punch of the same exact polymer was set aside for PIGE analysis as the pristine sample.

For cell assembly for the lithium isotope-exchange experiment, a chunk of ^{6}Li metal (95%, Cambridge Isotope Laboratories) suspended in mineral oil was rinsed with hexane (anhydrous, 95%, Aldrich), cut with a spatula to expose shiny nonoxidized Li metal, then flattened between two polypropylene sheets to yield a reflective and flat sheet of ^{6}Li. This sheet was punched into a 1/2″ diameter electrode, which was also rinsed with hexane, then when dried placed into a 2032 type coin cell (MTI corp.). The swelled polymer composite was placed on the ^{6}Li electrode. On top of the composite polymer was placed a natural isotopic (92.4% ^{7}Li, 7.6% ^{6}Li) Li electrode, prepared similarly to a reflective finish (without hexane washing) from Li foil (99%, 0.75 mm thick, Alfa Aesar). The cell was sealed with a stainless-steel spacer and wave spring, then exposed to a galvanostatic hold of 0.063 mA (0.05 mA/cm^2), where $^6Li^+$ were stripped from the ^{6}Li electrode and plated onto the ^{7}Li electrode. The low rate was chosen to avoid entering a mass transport limited regime with regard to Li^+ movement through the composite electrolyte.

The cell was run until it experienced erratic voltage behavior, after which the galvanostatic hold was stopped. The cell was disassembled, and the composite was rinsed with tetrahydrofuran (anhydrous, 99.9% inhibitor free, Aldrich) and allowed to dry.

Standards and samples were sealed within thin plastic sealable bags to prevent air contact and attached to PIGE sample stub holders. Care was taken to ensure that the portion of the ^{6}Li exchanged composite that was in contact with the electrodes was centered on the target stub, so that the PIGE beam spot (about 1 cm diameter) only hit the exchanged portion of the sample.

PIGE analysis was performed in the Nuclear Science Laboratory at the University of Notre Dame, targeting each sample ex vacuo with a 3.9 MeV beam of protons at ∼15 nA for 180 s to produce gamma-rays.[37] The resulting gamma-rays were measured using a high purity germanium detector (HPGe) (Canberra, 20%) located at approximately 75° to the beam. The proton beam at Notre Dame was produced by an NEC 9S tandem accelerator. The beam current was measured before and after each sample measurement, and the 770 keV gamma-ray from Argon-40 in the atmosphere was used to normalize the beam on target for each measurement.[38] Two gamma-rays at 429 and 478 keV, characteristic of the decay of the ^{7}Li nucleus, were background-subtracted and integrated to determine the total lithium concentration.

PIGE spectra for each sample and standard were collected, and the counts associated with the ^{7}Li(p,p′ γ)^{7}Li reaction were integrated over 474 to 485 keV to yield the intensity values used for building the calibration curve, where the measured intensity is plotted vs the known ^{7}Li content of the material. Included in building the calibration curve is the pristine PTHFDA-x-LiSTFSI composite electrolyte. Based on the intensity measured for the ^{6}Li exchanged composite, a value of remaining ^{7}Li is determined.

RESULTS

This work studies six crosslinked, lithiated SIPE systems gelled in PC and TEG. These six samples were based on the macromonomers PEGDA, PTHFDA, and PDMSDA crosslinked with KSTFSI, as pictured in Figure 1. Following

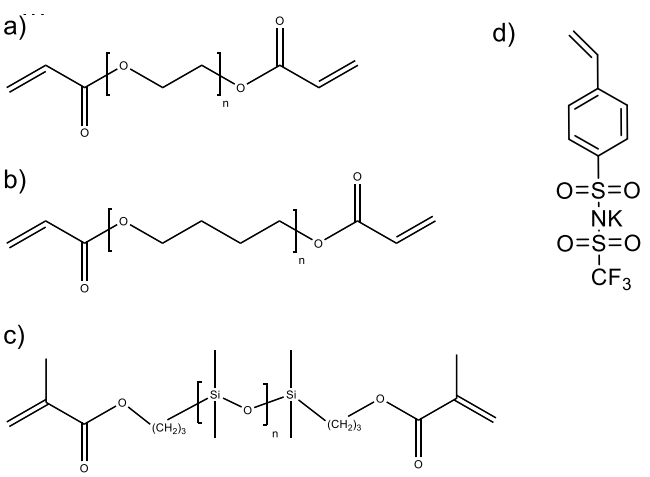

Figure 1. Molecular structure for the employed macromonomers and ionic monomer. (a) PEGDA (b) PTHFDA; (c) PDMSDA; and (d) KSTFSI.

crosslinking, the electrolytes were ion-exchanged to the lithium form as delineated in the Experimental Section. Each of these systems was studied in the pure and composite forms.

Three macromonomer structures were chosen to investigate the changes in ionic complexation and ion transport behavior of composites in the varying systems. These three systems have different dielectric constants/polarities, which, as will be shown, influences a variety of PE properties. The dielectric constants of the crosslinking macromonomer repeat units and of the solvents are outlined in Table 1. See the Supporting Information for more on the properties of the macromonomers.

Ionic Conductivity. Ionic conductivity in SIPEs is defined by eq 1, where eq 2 gives a more generalized definition for systems with a distribution of conducting species with varying mobility.[19]

https://doi.org/10.1021/acsapm.1c01535
ACS Appl. Polym. Mater. 2022, 4, 1095−1109

Table 1. Dielectric Constants of the Crosslinking Macromonomer Repeat Units and Organic Solvents

component	PEG	PTHF	PDMS	PC	TEG
dielectric constant	7.4[19]	5.0[39]	2.8[39]	65[40]	7.8[41]

$$\sigma = nq\mu \tag{1}$$

$$\sigma = \sum_{i} n_i q_i \mu_i \tag{2}$$

Here, n is the number of charge carriers, q is the charge of the ion, and μ is the mobility of the ion. The conductivity of gelled composite and pure PE samples with varying polymer chain chemistry are shown in Figure 2 to ascertain how backbone chemistry affects ion transport.

PEGDA-based polymers are the most commonly studied PE in this set of samples, and the results seen here are similar to those seen in other studies.[11] The PEGDA-based polymers perform with a slightly higher conductivity in PC as compared to the TEG gelled systems, and the addition of LICGC in both cases increases the conductivity only marginally. PEGDA-based polymers have a higher dielectric constant than both PTHFDA- and PDMSDA-based polymers, as seen in Table 1, and PEGDA electrolytes performed with a lower conductivity than both other polymer chain chemistries in this study, with the exception of the PDMSDA-x-LiSTFSI-LICGC-PC sample. This is a reproduction of trends seen in our previous work on SIPEs in which PTHFDA-x-LiSTFSI outperformed PEGDA-x-LiSTFSI in the gelled state due to a beneficial shift from polymer-coordinated cation states to higher mobility solvent coordinated cation states, as SIPEs with less polar polymer chains have fewer Li^+ solvation sites.[19]

The pure and composite PTHFDA-x-LiSTFSI samples have the highest conductivity in both the PC and TEG gelled states. In both solvents, the PTHFDA-x-LiSTFSI-LICGC has a conductivity about half an order of magnitude higher than the pure sample, indicating a potential difference in ion transport properties in the presence of LICGC. This significant enhancement of conductivity with inclusion of LICGC only occurs in the PTHFDA-based polymer, which hints at the importance of the crosslinking macromonomer chemistry on inorganic-ion-polymer interactions.

The performance of the PDMSDA-based samples depends heavily on the solvent environment. In the PC swelled system, the PDMSDA-x-LiSTFSI-LICGC-PC has a conductivity of about 2 orders of magnitude lower than the PDMSDA-x-LiSTFSI-PC. Swelling degree measurements (Supporting Information Table S1) revealed that the PDMSDA-x-LiSTFSI-LICGC sample exposed to PC only increased in mass by about 53% on average as compared to PDMSDA-x-LiSTFSI gelled in PC, which increased in volume by about 61.7%. As a benchmark, the PEGDA- and PTHFDA-x-LiSTFSI-LICGC masses increased by 222 and 125% respectively, in PC. With poor solvent uptake, the cations are less likely to be solvated, making ion transport within the PDMSDA-x-LiSTFSI-LICGC-PC system more difficult. In addition, the inaccessibility of the ether oxygens on the PDMS repeat unit make Li^+ coordination with the polymer chain unfavorable, further inhibiting ion transport. As will be discussed in greater detail later in this article, the sequestering of ion groups during polymerization on the inorganic particle surface, in addition to the potential frustrated segmental dynamics imposed by the particles, makes it likely that PC is unable to effectively penetrate the PDMSDA composite. With a high dielectric constant of about 65, the dielectric mismatch between PC and PDMSDA can only be overcome if the ionic groups are accessible to coordinate with the PC molecules. Indeed, the PDMSDA monomer is immiscible with PC. In contrast, TEG, being of low dielectric constant, can penetrate the PDMSDA network with or without the aid of accessible ionic groups for coordination, evidenced by the fact that TEG can dissolve PDMSDA monomers and that the PDMSDA conductivity in TEG is still higher than that of PEGDA-based SIPEs.

The PC gelled conductivity data are further normalized in terms of molar conductivity as well as intrinsic conductivity, where the former isolates the impact of ion mobility on experimental conductivity and the latter takes into account the volume of the composite occupied by the inorganic particles to produce the intrinsic conductivity of the polymer phase. The results are presented in Figure S1. The trends observed in the experimental conductivity are maintained in both normalizations, i.e., the large increase in conductivity from including LICGC in the PTHFDA PE. Intuitively, the PDMSDA-x-LiSTFSI-LICGC-PC sample has low ion mobility, as few solvent molecules are available to produce highly mobile solvent−ion complexes. Notably, we also produce the same results as Merrill et al., where the intrinsic conductivity of

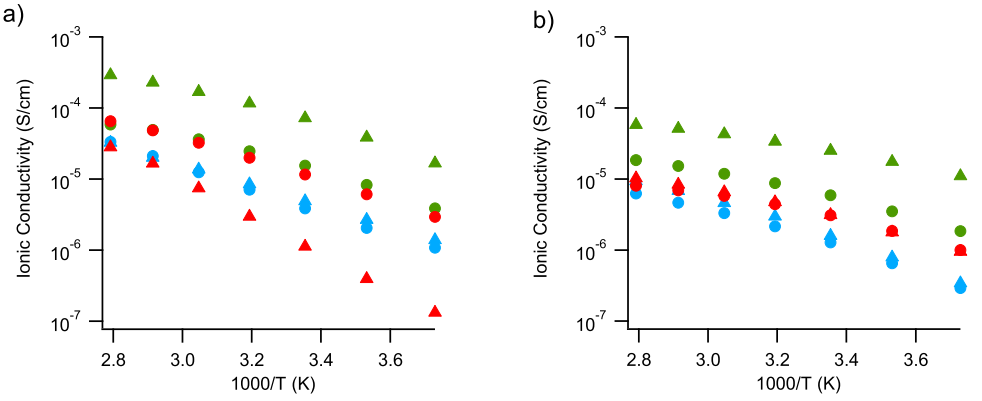

Figure 2. Ionic conductivity (S/cm) of pure and composite crosslinked SIPEs swelled in (a) PC and (b) TEG, represented by the following symbols: blue triangle, PEGDA-x-LiSTFSI-LICGC; blue circle, PEGDA-x-LiSTFSI; green triangle, PTHFDA-x-LiSTFSI-LICGC; green circle, PTHFDA-x-LiSTFSI; red triangle, PDMSDA-x-LiSTFSI-LICGC; red circle, PDMSDA-x-LiSTFSI.

https://doi.org/10.1021/acsapm.1c01535
ACS Appl. Polym. Mater. 2022, 4, 1095−1109

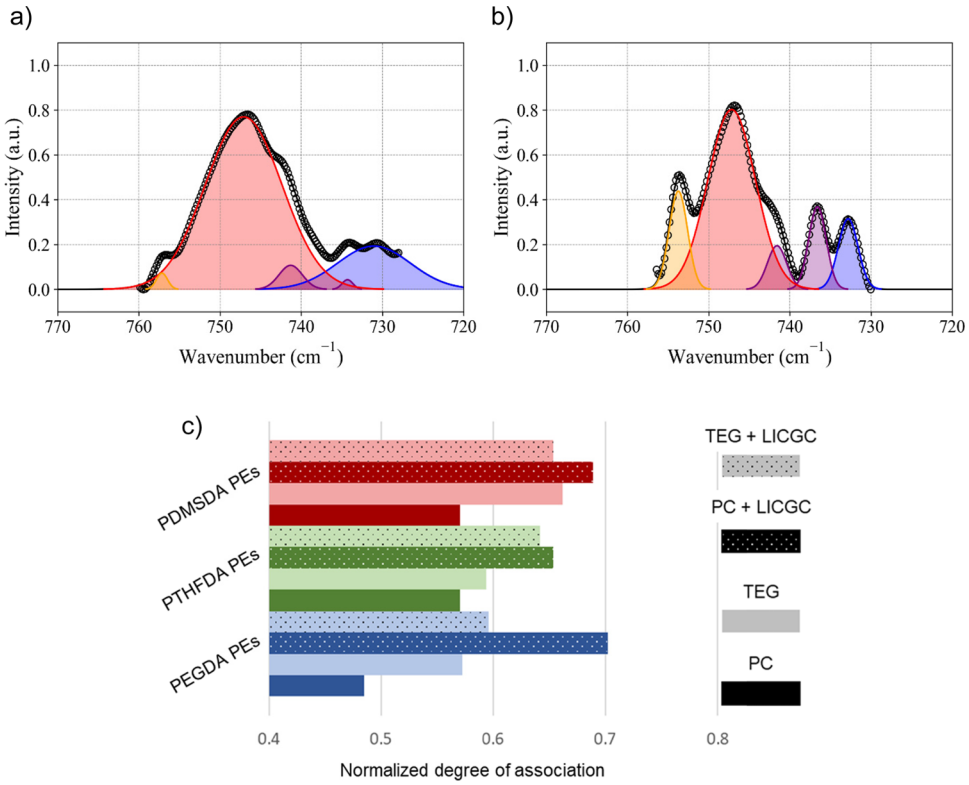

Figure 3. Raman spectra for the PC gelled (a) pure and (b) composite PTHFDA samples showing the association and dissociation peaks for the STFSI$^-$ breathing mode. The peak color indicates the degree of association, blue is full dissociation, purple is intermediate coordination species, red is full association, and orange is densely agglomerated species. (c) The overall normalized state of association, with 1 being the densest possible state, for each sample.

PEGDA-x-LiSTFSI-LICGC PEs is higher than that of the noncomposite analogues.[11]

The experimental conductivity data are fit by either the Arrhenius dependence or the Vincent−Fulcher−Tamman (VFT) dependence (eq S4 and eq S5, respectively) to quantify the difference in ion transport activation energy. The fitted parameters and the 25 °C ionic conductivities are presented in Table S2. The presence of a good solvent, such as PC, generally increases the prominence of solvent vehicular transport, decoupling ion transport from polymer relaxation and causing Arrhenius behavior.[19] However, the PTHFDA-based samples gelled in PC show VFT behavior, which indicates the coupling of conduction with a relaxation process. The fitted conductivity plots are presented in Figures S2 and S3 for reference.

The activation energy trends in this set of data confirm the generally positive impact of the inorganic particles on the ion transport within the system: the inclusion of LICGC decreases the ion conduction activation energy in all the samples except the PDMSDA-based samples. With the addition of LICGC, the T_0 value (related to the glass transition temperature T_g) increases, suggesting an increase in the apparent glass transition temperature. Generally, a decrease in segmental motion correlates with a decrease in conductivity. However, the conductivity in the composites increases despite the higher T_0, hinting at the possibility that ion conduction is de-coupled from bulk polymer relaxation dynamics. This result suggests the direct role of the inorganic particles in lithium-ion transport, as the ions must gain enhanced transport from interaction with the LICGC.

Raman-Driven Assessment of Ion Coordination. These general observations are further understood in correlation with the anion dynamics in the Raman data. As discussed, the Raman data show the relative population densities of the tethered anions in their various association states. The Raman peak wavenumbers are physically associated with the ion's degree of spatial freedom, and the STFSI$^-$ signals occur at similar wavenumbers as TFSI$^-$ signals, a common liquid electrolyte free anion.[31] The degree of freedom of the anion indicates the degree of coordination it is experiencing, where high degree of freedom at 730 cm^{-1} indicates complete dissociation, and low degree of freedom at 748 cm^{-1} indicates full association. Peaks in between these values are considered intermediate coordination states, and peaks beyond 748 cm^{-1} are tightly agglomerated species.[11,19,31,36,42−47] The intermediate coordination species are interpreted as states with loose coordination in various solvent shells, where coordination increases as the wavenumber approaches 748 cm^{-1}. The LICGC particles are expected to introduce new intermediate states, since the particle's negatively charged surface can attract lithium cations and form new anion-lithium-LICGC coordination species.[11] This prediction was found to be true in the TEG gelled systems. These species are also more likely to form densely packed agglomerates, so it is also expected that coordination species population will shift toward full association with the attractive LICGC surface encouraging closer association of ions in its vicinity, and this prediction was found to be true in the PC gelled systems.

The interpretive power of this diagnostic is not strong enough to determine the geometry or composition of each

https://doi.org/10.1021/acsapm.1c01535
ACS Appl. Polym. Mater. 2022, 4, 1095−1109

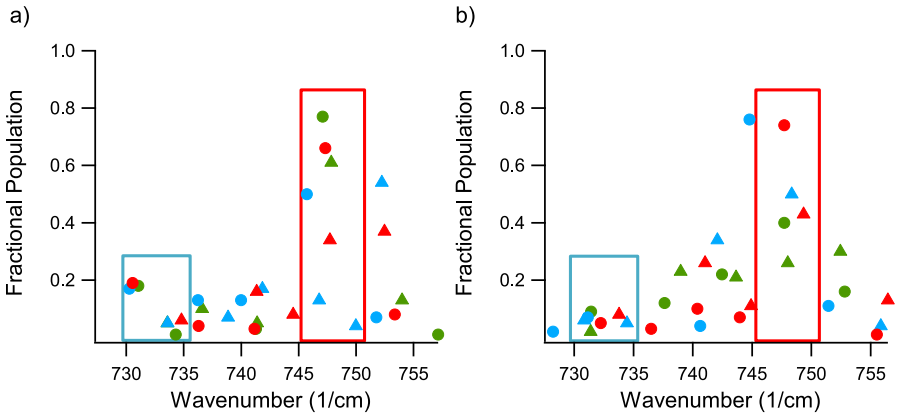

Figure 4. The fractional population is derived from the integration of the $STFSI^-$ Raman breathing peaks and is plotted against the excitation wavenumber for samples gelled in (a) PC and (b) TEG. The boxes indicate the fully associated wavenumber region (red) and the fully dissociated wavenumber region (blue), and the samples are denoted as follows: blue triangle, PEGDA-x-LiSTFSI-LICGC; blue circle PEGDA-x-LiSTFSI, green triangle, PTHFDA-x-LiSTFSI-LICGC; green circle, PTHFDA-x-LiSTFSI; red triangle, PDMSDA-x-LiSTFSI-LICGC; red circle, PDMSDA-x-LiSTFSI.

peak's coordination state.[48] However, the area under each peak can quantify the relative distribution of dissociated and associated anions, assuming that the Raman peak intensity for each state is equivalent. The following analysis to describe coordination behavior of the various polymers will build upon these population distributions. Figure 3a,b shows representative Raman spectra fitted using a Python Gaussian curve fitting program. The remaining fitted plots for the other compositions are found in Figures S4−S23. Using a population normalized linear weighting analysis, the total degree of anion association in a given sample can be obtained. As can be seen in Figure 3c, inclusion of the LICGC shifts anion populations toward higher degrees of association in all cases but one.

Beyond looking at the total degree of association, the nuance of the distribution of association states (low, moderate, high) sheds additional light on the environment experienced by anions in these polymer electrolytes. Figure 4 plots the peak wavenumbers versus the fractional population for all samples to depict the population distribution clearly.

The polymer samples gelled in PC trend toward full anion association and tight anion agglomeration, with high fractional populations of association states above 745 cm^{-1} as shown in Figure 4a. The pure polymers have lower population of tight agglomeration in all variants implying that the addition of LICGC universally alters the way the materials interact and are distributed within the polymer. More specifically, in the case of the PTHFDA-based ionomers, PTHFDA-x-LiSTFSI-LICGC-PC had two association states in the intermediate range (735−745 cm^{-1}) as compared to the one intermediate state seen in the PTHFDA-x-LiSTFSI-PC sample. PTHFDA-x-LiSTFSI-LICGC-TEG also has a higher fraction of anions in the intermediate state than the PTHFDA-x-LiSTFSI-TEG sample. The addition of an intermediate coordination state could contribute to the difference in conductivity, where the ionic conductivity of the composite is about half an order of magnitude higher than the LICGC-free polymer.

In addition to increased number of intermediate association states, the PTHFDA-x-LiSTFSI-LICGC gelled in PC also has both higher population density of fully associated ions (745−750 cm^{-1}) and lower population density of tightly agglomerated ions (>750 cm^{-1}) as compared to the composite PEGDA- and PDMSDA-based composite ionomers which show lower full association and higher tight agglomeration of ions. As compared to the pure ionomer samples, all the composite variants show higher populations of tight agglomeration (>750 cm^{-1}) with the addition of the inorganic particles. The pure ionomers all have summed fractional populations of ion speciation above 50% in the full association range (745−750 cm^{-1}), while composite ionomers shift ion association toward tighter states. This could be a performance limiting characteristic, as tight agglomeration logically hinders the conductivity of lithium through the system, as seen in our previous study of SIPEs.[49] Even so, we see an increase in conductivity in the PTHFDA-based composite samples with high association, plausibly indicating that the anion freedom is limited sterically by its interaction with an LICGC particle surface rather than by its presence in an isolated ionic aggregate in the bulk, where in the former lithium conduction might be favored and in the latter discouraged. The two opposing scenarios are not seen in pure SIPEs; however, the LICGC introduces a new way in which high anion association can lead to higher conductivity.

The majority of anions in the pure PC gelled samples are either fully dissociated (730−735 cm^{-1}) or fully associated (740−745 cm^{-1}). With the addition of LICGC, the PC samples exhibit a shift toward higher association. The composite samples gelled in TEG show a shift toward looser association, with population distribution of the ionic association states, shown in Figure 4b, concentrated in the intermediate coordination region. There is a large gap between the dielectric constant of PC and the PTHFDA/PDMSDA macromonomers and, therefore, reduced miscibility between PC and those polymer chains, whereas TEG has a dielectric constant like those of the macromonomers. This allows the TEG to easily penetrate the polymer electrolytes and dissociate anion-cation pairs. As a result of this property, the PDMSDA polymers have lower population density of tightly agglomerated ion states and higher population density of intermediate association states in the TEG gelled state.

As seen most prevalently in the TEG gelled PTHFDA-based ionomers, full dissociation and tight agglomeration are weak contributors to the total coordination state populations; rather, a wide range of intermediate coordination states are strongly represented. In PC, LICGC brings a shift toward full and tight

https://doi.org/10.1021/acsapm.1c01535
ACS Appl. Polym. Mater. 2022, 4, 1095−1109

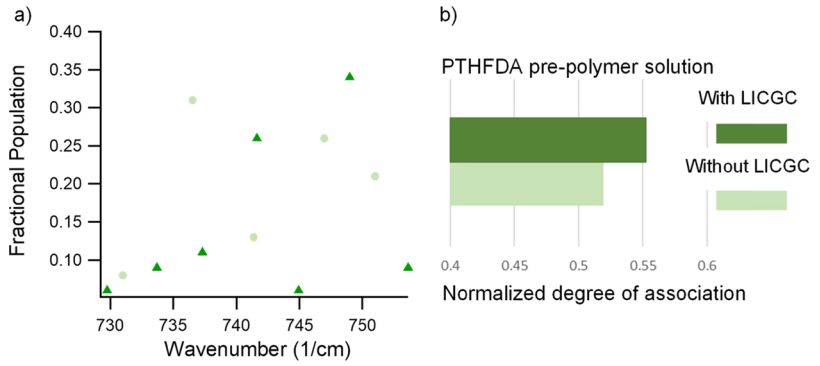

Figure 5. (a) Fractional populations associated with each set of ion coordination states are plotted against the Raman wavenumber. The data points represent pure PTHFDA pre-polymer solution (circle) and composite PTHFDA pre-polymer solution (triangle) in TEG. (b) Overall normalized state of association, with 1 being the most associate stated, for each sample.

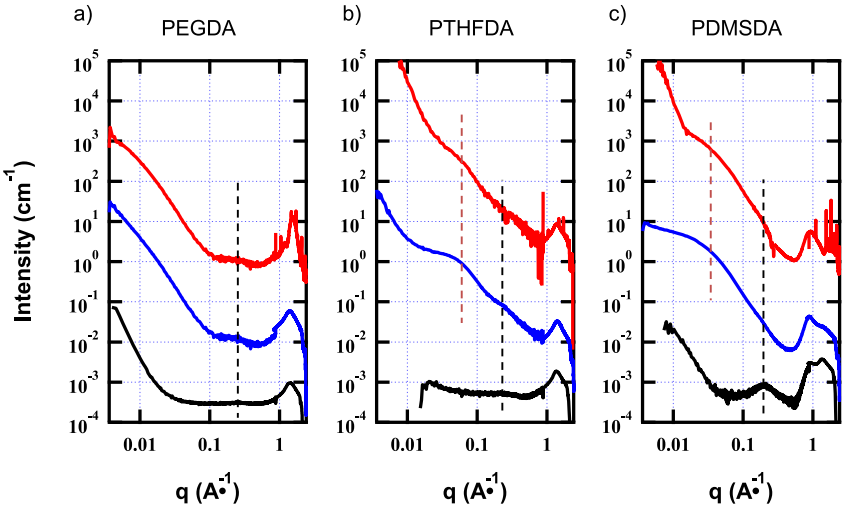

Figure 6. SAXS/WAXS profiles of (a) PEGDA-based, (b) PTHFDA-based, and (c) PDMSDA-based networks of varying composition gelled with PC. The polymer samples are represented by the following: black line, homopolymer; blue line, x-LiSTFSI; and red line, x-LiSTFSI-LICGC.

association. While the presence of LICGC is observed differently in the correlation dynamics of the two solvents, the addition of LICGC generally increases the conductivity of the sample, if only marginally in the cases of the PEGDA-based sample. The results in Figure 4 support a scenario in which the inorganic particles create an environment that alters the transport behavior of the cation, where medium to high states of anion coordination appear favorable in conductivity performance, possibly through stabilization of anion or cation solvation states with the particle surface. We hypothesize that the inclusion of the LICGC drives the ionic monomers to the surface of the particle, which can lead to different ion transport dynamics due to different ion distribution in the CPEs compared to the LICGC-free polymers. The driving force of the inorganic particle−ion interactions appear to depend on the crosslinking macromonomer chemistry. The exact motion of the lithium, distribution of electrolyte components, and associability of the lithium with LICGC are still unclear but probed in the following sections.

Investigation of the Inorganic Particle−Ion Interaction in Pre-Polymer Solution. Previous work investigating the interfacial compatibility in composite ionomers has shown high resistance between the components; therefore, it is unknown whether the LICGC surface can interact with the ions in the way proposed herein. To test our proposal, the solution of reactants for the PTHFDA-based ionomers was probed prior to polymerization. The comparison of the PTHFDA solutions with and without LICGC (Figure 5) shows that the anions in the solution without LICGC trend toward dissociation, while anions in the solution with LICGC trend toward association, indicating that the ionic monomers in the solution are interacting with LICGC particles. From these results, we theorize that the PTHFDA pre-polymer solution is acting like a soggy-sand electrolyte, where ionic groups are driven to the LICGC particle surface to produce an ion-rich space-charge domain.[30,32,33] Under the right conditions (some of which are similar to those studied here), it has been well documented that such space-charge regions can become percolated through the electrolyte, resulting in a long-range semistable structure to which the enhanced conductivity of such electrolytes is attributed. Here, that long-range structure is preserved during the crosslinking polymerization process, becoming locked in place to produce a CPE with enhanced conductivity. This theory is explored in more detail later in the manuscript.

Structural Analysis via SAXS/WAXS. As a technique particularly well suited to the study of structure of soft materials, SAXS/WAXS is used to probe the composite polymers studied here.[50] Interpretation of SAXS/WAXS spectra of similar ionic gel polymers by our research group

https://doi.org/10.1021/acsapm.1c01535
ACS Appl. Polym. Mater. 2022, 4, 1095−1109

has established transport-structure relationships and shown that different crosslinking macromonomer chemistry can influence network structure.[49,51] Specifically of interest to the present study is whether the changes in ion transport behavior observed with the inclusion of the LICGC particles stems from any nanostructural changes in the polymer. It is possible that inclusion of the LICGC particles could alter backbone or ionic cluster correlations via interactions between monomers and the particle surfaces, leading to changes in ion transport. Such differences could be visible with SAXS/WAXS. Longer-range structural coordination, on the scale of the particle size (upper micrometer range) are not as easily discernable with SAXS/WAXS in the presence of the inorganic particles.

Scattering profiles of three compositions for each crosslinking macromonomer are studied: the homopolymer form (pure crosslinked macromonomer), the ionomer form (crosslinking monomer co-polymerized with STFSI) and the composite (ionomer + LICGC). Further, each of these compositions is examined in the dry, TEG gelled, and PC gelled states.

Figure 6 shows the SAXS/WAXS profiles of the core set of polymers gelled in PC, separated by crosslinking macromonomer, a representative subset of all the SAXS/WAXS profiles. SAXS/WAXS profiles for the other compositions are presented in Figures S24−S26. The crystalline peaks of the LICGC are visible in the WAXS region of the LICGC containing composites. All compositions of all three sets of materials exhibit a correlation peak around 0.21 $Å^{-1}$, which is marked with the vertical dashed black line. Using the Bragg condition, where the distance d_x between the correlating structures is given by eq 3, this distance d_x is about 3.0 nm.[52] As this correlation peak is present in all samples, including the homopolymers, it is assigned to the acrylate backbone correlation.

$$q_x = \frac{2\pi}{d_x} \tag{3}$$

This result, the correlation distance of the acrylate backbone, agrees perfectly with our previous results studying PEGDA-based ionomers of the same molecular weight.[49] Further, it indicates that inclusion of the LICGC particles does not alter backbone correlation for these compositions.

With the acrylate backbone assigned, other features that are not present in the homopolymer spectra but that are in the ionomer or composite ionomer spectra may be attributed to the presence of the ionic groups. In the PEGDA-based samples, at the low charge densities of these ionomers the ionic correlation peaks may not be visible, or may overlap the acrylate peak.[49] Peaks assigned to ionic cluster correlations, indicated by the vertical dashed red lines, in the PTHFDA- and PDMSDA-based samples are at 0.049 $Å^{-1}$ (12.8 nm) and 0.035 $Å^{-1}$ (18.0 nm), respectively. The large correlation distances in these ionomers may represent a significant phase separation between the ionic LiSTFSI groups and the polymer backbone/crosslinkers, a result perhaps not surprising given the difficulty in achieving a single-phase pre-polymer solution for the lower dielectric constant crosslinking macromonomers. In our previous work, we did not observe low/mid q ionic correlations until high charge density (mol of charge relative to total mass of polymer) samples were studied; however, we also did not examine samples with low charge densities and low dielectric crosslinking macromonomers such as those in the present study. This result may hint at diverse phase behavior for some of these samples, especially the PTHFDA-based ionomers, where low and high charge densities yield longer ion correlation distances and moderate charge density yields less phase separation.

The LICGC particles do not appear to alter the nanoscale structure of the polymers investigated above. If the LICGC does alter the network structure, the impact must be larger than the q space accessible with SAXS/WAXS, such as formation of long-range percolated ion domains, encouraged by the presence of LICGC, that span the thickness of the gel composite. This theory is supported by literature studies on "soggy-sand" electrolytes that incorporate inorganic fillers in liquid electrolyte where such percolation is observed.[30,32,33] This theory is further tested later in this article.

Probing Li^+ Conduction Pathways. Given the unique conductivity performance of the PTHFDA composite polymers, and the multitude of possible ion transport mechanisms in these systems, identifying the dominant ion transport mechanism would lead to insights for high-performance electrolyte design. From the literature, when the LICGC loading is high (77%) and sintered prior to backfilling with polyethylene oxide (PEO), a continuous inorganic phase enables ion transport through the inorganic domain.[1] In other cases, where the LICGC loading is low to moderate and nonsintered, much like the materials in the present study, it has been proposed that discontinuity of the particles likely causes the majority of ion transport to occur in the polymer phase.[11] Further, at least for conventional gel polymer materials like PEO or PEGDA-based networks, it has been shown that a high activation energy barrier exists for moving active ions between the polymer and inorganic phases.[9,53]

If Li^+ transport is taking place through the highly conductive LICGC particles, the overall high conductivity of the PTHFDA-x-LiSTFSI-LICGC could be explained. To rule out this possibility, an experiment was devised that would determine where Li^+ transport was taking place in this composite. PIGE spectroscopy is an established ion beam analysis technique capable of element specific quantification, based on gamma emission from nuclei excited via a particle accelerator generated proton beam. As a compliment to particle-induced X-ray emission (PIXE), PIGE is especially well suited to detection of lighter elements. The use of PIGE to study battery materials is gaining traction in the analysis of Li interfaces and other kinds of electrolytes, yet to our knowledge, this technique has not been used to interrogate Li^+ conduction pathways.[54]

For detection of Li, PIGE is sensitive to the specific isotope, where ^7Li is detected via the $^7Li(p,p'\gamma)^7Li$ reaction, which produces gamma emissions at 429 and 478 keV when the beam used is a proton beam (Figure S27). Under the same conditions, ^6Li does not emit gamma-rays at 429 or 478 keV, making ^6Li effectively invisible to PIGE at these energies.[55,56] To determine where Li transport occurs in the PTHFDA-x-LiSTFSI-LICGC sample, a simple experiment was designed where the ^7Li content of the pristine composite is measured and compared to a composite where the Li has been exchanged electrochemically to ^6Li. Based on how much ^7Li remains in the treated composite, Li^+ transport pathways can be inferred.

A sample of the PTHFDA-x-LiSTFSI-LICGC was assembled in a coin cell containing a ^6Li metal electrode on one side, and a standard (predominantly ^7Li) electrode on the other side. A constant, small current was applied across the cell, to induce dissolution of the ^6Li electrode and deposition

https://doi.org/10.1021/acsapm.1c01535
ACS Appl. Polym. Mater. 2022, 4, 1095−1109

of Li on the ^{7}Li electrode, in an effort to replace the mobile Li in the composite electrolyte with ^{6}Li. The galvanostatic condition was held 9.1 times longer than theoretically required to replace all Li in the composite, meaning all mobile Li was likely exchanged from ^{7}Li to ^{6}Li.

A set of standards were prepared to enable quantification of the ^{7}Li in the composites. These standards are homopolymers made from the PTHFDA monomer and known amounts of LICGC, ensuring the matrix of the standards matches that of the samples. Based on a LICGC stoichiometry of $Li_{1.5}Al_3Ti_{1.7}Si_2P_{2.8}O_{12}$, the known ^{7}Li content of the standards and the intensity of emissions measured from PIGE is used to build a calibration curve (Figure S28).[57] Using the calibration curve, the content of ^{7}Li remaining in the composite after ^{6}Li replacement is measured. Further details are in the Experimental Section and the SI.

Figure 7 shows the weight % of ^{7}Li in the pristine composite and the fractional contribution of the different Li containing

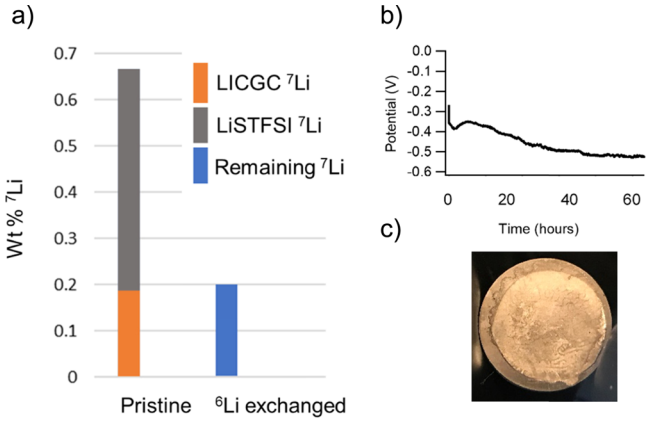

Figure 7. (a) Weight % of ^{7}Li in pristine composite and composite after ^{6}Li replacement. (b) Potential of the ^{6}Li replacement galvanostatic hold. (c) Photograph of the electrode plated with ^{6}Li.

components (polymer phase LiSTFSI and LICGC) to that total, as well as the ^{7}Li remaining in the composite after ^{6}Li replacement. Additionally, the potential during the galvanostatic hold and a photo of the plated ^{6}Li are shown, indicating stable deposition of ^{6}Li took place. Note, in this configuration the electrolyte consists only of the composite gelled with PC, meaning there is no free salt, and the composite is a single-ion conductor with all Li hosted within the composite.

The amount of ^{7}Li remaining in the ^{6}Li exchanged composite is almost exactly equal to the ^{7}Li initially present in the LICGC, where the exchanged composite has 0.20 wt % ^{7}Li remaining and the initial LICGC contribution is 0.18 wt % ^{7}Li. Given that the composite was subjected to ^{6}Li replacement for 9.1 times the amount of time theoretically required to replace all Li in the material, it is safe to say that the remaining ^{7}Li is not mobile. These results suggest that the Li present in the LICGC is not mobile in these composites, or if it is mobile, it contributes negligible Li^+ flux compared to the polymer phase. As is such, Li^+ does not appear to move through the LICGC particles nor between the inorganic and polymer phases. This conclusion is supported by conductivity analysis of a homopolymer PTHFDA composite, where the only source of Li is from LICGC. Figure S29 shows the conductivity of this material gelled with TEG, where the conductivity is over an order of magnitude lower than PTHFDA-x-LiSTFSI-LICGC, but an order of magnitude higher than TEG. These results indicate that while there is a Li^+ conduction pathway through the particle phase, the contribution to total Li^+ flux is negligible. Further discussion is found in the SI.

The predominant ion transport mechanism in the PTHFDA-x-LiSTFSI-LICGC composite must therefore be through the polymer phase or along the surface of the LICGC particles through an ion-rich domain. As the inclusion of the LICGC improves the conductivity, the latter option seems likely.

Unified Theory of LICGC Impact on Polymer Structure and Ion Transport. The experiments so far have probed the nature of the LICGC's inclusion within the ionomer materials to define the inorganic particle's ability to support cation conduction and its effect on ionomer conformation and structure. As a combined body, the conductivity, Raman, scattering, and PIGE results indicate the creation of a long-range percolated inorganic−ionic domain that can enhance ion conduction, as modulated by the dielectric constant of the polymer crosslinker.

Review of the conductivity analysis and Raman coordination studies reveals an indirect correlation between the level of agglomeration and conductivity. As the population density of tightly agglomerated states increases, the conductivity decreases, which is shown in the pure and composite PDMSDA- and PEGDA-based ionomer samples as compared to the PTHFDA-based samples. The TEG swelled polymer coordination dynamics highlight the importance of intermediate states of association (735−745 cm^{-1}) for cation conduction. The high extent of intermediate association in the TEG gelled PTHFDA-based ionomers in conjunction with the higher differential in conductivity between the PTHFDA-based samples and the other samples in TEG as compared to PC, where there is lower intermediate coordination, highlights the importance of these loosely bound association species. Further, the Raman shows that the influence of LICGC on the anion association states is present in the pre-polymer solution, meaning the LICGC impacts the final polymer−ion domain arrangement.

The SAXS data supports previously reported evidence of phase separation between the anion and bulk polymer regions in ionomers and revealed little difference in short-range structure due to the addition of LICGC. With observed inorganic−cation−anion interactions seen in the Raman analysis, as mentioned, LICGC may be introducing a long-range structure with the tethered anions ordered preferentially around the percolated inorganic particles to create an enhanced ion conductive channel within the polymer bulk of the PTHFDA-x-LiSTFSI-LICGC electrolyte, as depicted in Figure 8c. Figure 8a shows the proposed LICGC−ionic monomer interaction responsible for the ion-rich phase formation. The ion-rich space-charge domain at the particle surface would give continuous support to lithium transport, as the tethered anions and negatively charged LICGC surface would all stabilize the dissociated traveling cation. The lowering of ion transport activation energy in composite samples supports this theory. PIGE additionally confirmed that little to no conduction occurs through the LICGC phase, so the idea of percolated surface-facilitated travel is the most fitting prediction with the data provided.

Figure 8 illustrates the less polar PTHFDA crosslinking monomer, which has a slightly unfavorable interaction with the ionic monomer, driving coordination between the ionic

https://doi.org/10.1021/acsapm.1c01535
ACS Appl. Polym. Mater. 2022, 4, 1095−1109

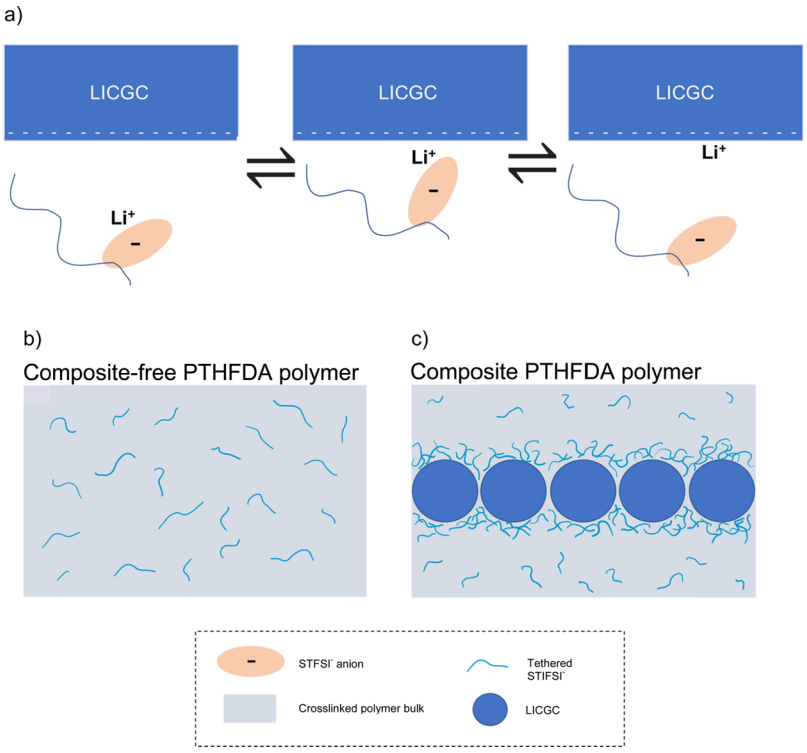

Figure 8. (a) Proposed nanoscale interaction between LICGC, lithium, and anion, where the LICGC particle is represented as an infinite plane as it is on the micrometer scale. (b) Proposed ion domain distribution in LICGC-free PTHFDA sample. (c) Proposed percolated inorganic and ion domain structure creating an ion channel beneficial for ion conduction.

monomer and particle surface as the ionic monomer seeks a more stable environment. The driving force is strong enough to produce LICGC−ionic monomer interaction (evidenced by the pre-polymer solution Raman spectra), but not strong enough to force all the ionic groups to the particle surface. This conclusion is supported by the low population of tightly agglomerated anions in the PTHFDA-x-LiSTFSI-LICGC Raman spectra and SAXS structural analysis. The resulting proposed structure, shown in Figure 8, is one that enables facile solvent penetration into the network but also produces a potentially percolated ion-rich domain at the LICGC surface which is apparently beneficial for ion conduction.

The formation of the beneficial percolated ion domains, assembled via the inorganic−ionic monomer interactions, is modulated by the crosslinking macromonomer, where there is a so-called "goldilocks" material space that leads to higher conductivity. PEGDA, having the highest dielectric constant of all the crosslinking macromonomers, does not drive the highly polar ionic monomer to interact with the LICGC surface; the ionic monomer and PEGDA monomers are stable in solution together. The lack of thermodynamic driving force for the LICGC−ionic monomer interaction results in a network with homogeneously distributed ion domains, similar to that of the noncomposite PEGDA electrolyte, explaining the small impact of LICGC on the conductivity of the PEGDA system. A schematized representation of the proposed PEGDA structure is presented in Figure S30.

The PDMSDA crosslinking monomer, with the lowest polarity and worst miscibility with the polar ionic monomer, causes a majority of the ionic monomers to reside at the LICGC particle surface. A schematized representation of the proposed PDMSDA structure is presented in Figure S31. Especially in PC, the Raman spectra of the PDMSDA-x-LiSTFSI-LICGC electrolyte indicate a large portion of the anions are in a tightly agglomerated state. Total sequestration of the ionic monomer at the particle surface in the PDMSDA case has at least two detrimental impacts on conductivity. Firstly, the network is unable to swell in PC, as the highly polar solvent is not able to penetrate the PDMSDA rich regions to reach the ionic domains, meaning there are few dissociated ions that can contribute to Li^+ flux. This idea is depicted in Figure S32. Secondly, the resultant ion domains are likely not percolated but instead may be isolated islands, where there is no continuous LICGC surface-mediated ion transport. As interpreted from the TEG conductivity data, where the LICGC and LICGC-free PDMSDA polymers behave similarly, it can be inferred that ion transfer from island to island is the limiting step and contributes ion conduction resistance.

Further Probing of the Proposed LICGC Impact on Li^+ Transport in PTHFDA Polymers. Taken as a whole, the results so far suggest the mechanism behind the enhanced conductivity of the PTHFDA-x-LiSTFSI-LICGC polymer. The improved conductivity is theorized to be a result of Li^+ diffusion across LICGC particle surfaces through a percolated ion-rich domain, a self-assembled structure arising from surface interactions mediated by the pre-polymer solution chemistry. To further test this theory, two additional experiments are performed. In the first, the solvent of the pre-polymer solution is changed from TEG to dimethylformamide (DMF). In the second, the surface area of the LICGC particles is varied.

DMF is a solvent of moderate polarity ($\varepsilon_{DMF} \approx 37$) that is capable of solvating both PTHFDA and KSTFSI monomers. The higher polarity of DMF compared to TEG (the standard pre-polymer solvent used in this study) allows for better stabilization of the ionic monomer as well as charge screening of the ionic monomer and LICGC surface. Figure S33 shows

https://doi.org/10.1021/acsapm.1c01535
ACS Appl. Polym. Mater. 2022, 4, 1095−1109

the conductivity of PTHFDA polymers prepared from DMF compared to those prepared from TEG. When PTHFDA-based polymers are prepared from a DMF based pre-polymer solution, the conductivity of the composite and inorganic-free electrolytes is nearly identical. With DMF facilitated charge screening in the pre-polymer solution, the LICGC particles do not impart a conductivity improvement, presumably due to lack of a percolated ion-rich domain stemming from minimal LICGC−ionic monomer interaction.

Secondly, if the mechanism of enhanced conductivity is related to LICGC−ionic monomer interaction, then changing the available LICGC surface area should impact the electrolyte performance. Figure S34 shows SEM images for pristine (about 1 μm diameter) and ball milled (about 60 nm diameter) LICGC particles. Figure S35 shows the conductivity of a variety of PTHFDA-based polymers with different surface area (but equivalent wt %) LICGC particles. When the particle diameter of the LICGC is reduced from about 1 μm to about 60 nm with ball-milling, the conductivity of PTHFDA composites using the nanoLICGC is lower than the PTHFDA-x-LiSTFSI-LICGC sample in PC, and equal to the composite-free PTHFDA sample in TEG. For the standard micron LICGC samples, there are roughly 340 ionic monomers per nm^2 particle surface area. That number drops to about 20 molecules per nm^2 for the nanoLICGC. Note these numbers are assuming all ionic monomer goes to the surface of the particle, which we have argued is not the case for PTHFDA samples. Apparently, increasing the surface area relative to the ionic monomer content disrupts the formation of percolated ion-rich domains; the ionic monomers may be spread too sparsely at the particle surfaces to provide a continuous space-charge domain beneficial for ion transport.

Figure S35 also shows conductivity data for PTHFDA-based electrolytes in which the ratio of ionic monomer to PTHFDA monomer is increased, yielding polymer electrolytes with a higher charge density. These high charge density polymers are likewise prepared with the standard LICGC and the nano-LICGC. The conductivity of the high charge density samples with micron LICGC is lower in both solvents than the inorganic-free high charge density PTHFDA electrolyte. The conductivity of the nanoLICGC samples is higher than the inorganic-free high charge density electrolyte. The high charge density micron LICGC sample has roughly 940 ionic monomers per nm^2 of particle surface area, while the nanoLICGC sample has roughly 50 ionic monomers per nm^2. Apparently, the beneficial ionic monomer to surface area ratio is not universal across particle size; however, considering the proposed percolated structure, nanosized particles would pack differently than micrometer-sized particles and result in more particle-particle junctions which could explain this discrepancy. Schematics for proposed ion domain-particle arrangement as a function of particle surface area and ion content are presented in Figure S36, and all 25 °C conductivities are listed in Table S3.

Notably, the PTHFDA-x-LiSTFSI-nanoLICGC sample in PC has a 25 °C conductivity of over 2×10^{-4} S/cm, which is above the requirement for suitable Li^+ transport for a practical electrolyte, a difficult milestone to achieve with SIPEs. There is certainly room for optimization on the monomer to surface area ratio, charge density, and LICGC content to further improve conductivity.

That the beneficial impact of the LICGC can be diminished by screening charges in the pre-polymer solution and by adjusting the ionic monomer to particle surface area ratio is further proof that the enhanced conductivity in certain PTHFDA composites stems from ion-particle interactions. This finding informs design metrics for high-performing composite electrolyte composition and processing, and warrants additional investigations, especially considering the complexity of the composition-performance relationships, where everything from pre-polymer solvent to particle size is important to consider.

CONCLUSIONS

This study constructs a fundamental description of ion transport and material configuration in composite polymer systems and specifically highlights factors that facilitate fast lithium conduction. In general, the composite ionomer gels exhibited higher conductivity than the pure ionomer gels, with a large performance enhancement seen in the composite PTHFDA-based samples. While LICGC is expected to raise the conductivity, this unexpectedly high jump in performance shows the proclivity of the PTHFDA-based system to high-performance interactions with LICGC and, in general, highlights the importance of macromonomer-anion-inorganic microstructure for fine tuning the proficiency of ion transport. Raman spectroscopy shows that the inclusion of LICGC alters the ionic environment, introducing additional states of anion conformational freedom. These states of anion freedom are dependent on crosslinking macromonomer chemistry and gelation solvent. In the high conductivity PTHFDA-x-LiSTFSI-LICGC samples and pre-polymer solutions, the presence of these intermediate anion states indicates particle−ionic monomer interactions that persist after polymerization. SAXS/WAXS spectra show that the effect of the LICGC on ionic monomer arrangement is long-range. Lastly, PIGE shows that the lithium does not travel through the volume of LICGC to a meaningful extent, so a percolated surface-mediated transport mechanism explains the enhanced conductivity in these composites.

We propose that the conductivity enhancement stems from the production of long-range, percolated inorganic/ion-rich channels, similar to what is observed in liquid soggy-sand electrolytes.[33] The degree of inorganic−ionic monomer correlation depends on the mismatch between the crosslinking macromonomer and ionic monomer polarity, which is further modulated by the effects of the pre-polymer casting solvent dielectric constant, as well as particle surface area and total ionic monomer content. With the proper combination of these factors, fast lithium-ion conduction is achieved via LICGC-assisted transport. The best material, which is unoptimized at this point, performed above the threshold for practical use and was made of easy to synthesize or commercially available materials. Ample space remains for optimization of the CPE compositions, including LICGC particle surface area and loading, CPE charge density, and exploration of additional crosslinking macromonomer chemistries or casting solvent. Such optimization, guided by the fundamental property-performance relationships established here, will lead to continued CPE conductivity enhancement.

ASSOCIATED CONTENT

Supporting Information

The Supporting Information is available free of charge at https://pubs.acs.org/doi/10.1021/acsapm.1c01535.

https://doi.org/10.1021/acsapm.1c01535
ACS Appl. Polym. Mater. 2022, 4, 1095−1109

Intrinsic and molar conductivity, Arrhenius/VFT fitting, additional experimental conductivity data, fit Raman spectra, ^{7}Li PIGE analysis and calibration curve, additional SAXS/WAXS spectra, additional long-range structural schematics, SEM images of LICGC particles (PDF)

AUTHOR INFORMATION

Corresponding Author

Jennifer L. Schaefer − *Department of Chemical and Biomolecular Engineering, University of Notre Dame, Notre Dame, Indiana 46556, United States;* orcid.org/0000-0003-4293-6328; Email: Jennifer.L.Schaefer.43@nd.edu

Authors

Emily S. Doyle − *Department of Chemical and Biomolecular Engineering, University of Notre Dame, Notre Dame, Indiana 46556, United States;* Present Address: Pritzker School of Molecular Engineering, University of Chicago, Chicago, Illinois 60637, United States

Hunter O. Ford − *Department of Chemical and Biomolecular Engineering, University of Notre Dame, Notre Dame, Indiana 46556, United States;* orcid.org/0000-0002-9510-0324

David N. Webster − *Department of Chemical and Biomolecular Engineering, University of Notre Dame, Notre Dame, Indiana 46556, United States*

Peter J. Giannini − *Department of Chemical and Biomolecular Engineering, University of Notre Dame, Notre Dame, Indiana 46556, United States*

Meghanne E. Tighe − *Department of Chemistry and Biochemistry, University of Notre Dame, Notre Dame, Indiana 46556, United States;* orcid.org/0000-0002-8930-892X

Robert Bartsch − *Department of Physics, University of Notre Dame, Notre Dame, Indiana 46556, United States*

Graham F. Peaslee − *Department of Chemistry and Biochemistry and Department of Physics, University of Notre Dame, Notre Dame, Indiana 46556, United States;* orcid.org/0000-0001-6311-648X

Complete contact information is available at: https://pubs.acs.org/10.1021/acsapm.1c01535

Author Contributions

The manuscript was written through contributions of all authors. All authors have given approval to the final version of the manuscript. E.S.D. and H.O.F. contributed equally.

Funding

The authors are greatly appreciative of the funding for this work from the National Science Foundation via award numbers CBET-1706370 (personnel, materials, and supplies) and CBET-2100811 (materials and supplies). HOF gratefully acknowledges additional funding from the Notre Dame Arthur J. Schmitt Foundation, The Notre Dame Center for Environmental Science and Technology Pre-doctoral Fellowship, and the Notre Dame Patrick and Jana Eilers Graduate Student Fellowship. This research used resources of the Advanced Photon Source, a U.S. Department of Energy (DOE) Office of Science User Facility operated for the DOE Office of Science by Argonne National Laboratory under Contract No. DE-AC02-06CH11357.

Notes

The authors declare no competing financial interest.

For purposes of modeling, the raw SAXS/WAXS spectral data are available upon request.

ACKNOWLEDGMENTS

The authors acknowledge the assistance of the Notre Dame Integrated Imaging Facility for use of the SEM and the Notre Dame Materials Characterization Facility for Raman Spectroscopy. Further, the authors acknowledge Dr. Xiaobing Zuo from the Argonne National Laboratory for assistance in collecting SAXS/WAXS data.

REFERENCES

(1) Palmer, M. J.; Kalnaus, S.; Dixit, M. B.; Westover, A. S.; Hatzell, K. B.; Dudney, N. J.; Chen, X. C. A Three-Dimensional Interconnected Polymer/Ceramic Composite as a Thin Film Solid Electrolyte. *Energ. Storage Mater.* **2020**, *26*, 242−249.

(2) Guan, X.; Wu, Q.; Zhang, X.; Guo, X.; Li, C.; Xu, J. In-Situ Crosslinked Single Ion Gel Polymer Electrolyte with Superior Performances for Lithium Metal Batteries. *Chem. Eng. J.* **2019**, *2020*, 122935.

(3) Wu, F.; Zhang, K.; Liu, Y.; Gao, H.; Bai, Y.; Wang, X.; Wu, C. Polymer Electrolytes and Interfaces toward Solid-State Batteries: Recent Advances and Prospects. *Energ. Storage Mater.* **2020**, *33*, 26−54.

(4) Dirican, M.; Yan, C.; Zhu, P.; Zhang, X. Composite Solid Electrolytes for All-Solid-State Lithium Batteries. *Mater. Sci. Eng. R Reports* **2019**, *136*, 27−46.

(5) Jiang, M.; Zhang, Z.; Tang, B.; Dong, T.; Xu, H.; Zhang, H.; Lu, X.; Cui, G. Polymer Electrolytes for Li-S Batteries: Polymeric Fundamentals and Performance Optimization. *J. Energy Chem.* **2021**, *58*, 300−317.

(6) Liu, J.; Pickett, P. D.; Park, B.; Upadhyay, S. P.; Orski, S. V.; Schaefer, J. L. Non-Solvating, Side-Chain Polymer Electrolytes as Lithium Single-Ion Conductors: Synthesis and Ion Transport Characterization. *Polym. Chem.* **2020**, *11*, 461−471.

(7) Yu, X.; Manthiram, A. A Review of Composite Polymer-Ceramic Electrolytes for Lithium Batteries. *Energ. Storage Mater.* **2021**, *34*, 282−300.

(8) Lee, Y. S.; Ju, S. H.; Kim, J. H.; Hwang, S. S.; Choi, J. M.; Sun, Y. K.; Kim, H.; Scrosati, B.; Kim, D. W. Composite Gel Polymer Electrolytes Containing Core-Shell Structured SiO2(Li+) Particles for Lithium-Ion Polymer Batteries. *Electrochem. Commun.* **2012**, *17*, 18−21.

(9) Chen, X. C.; Sacci, R. L.; Osti, N. C.; Tyagi, M.; Wang, Y.; Palmer, M. J.; Dudney, N. J. Study of Segmental Dynamics and Ion Transport in Polymer-Ceramic Composite Electrolytes by Quasi-Elastic Neutron Scattering. *Mol. Syst. Des. Eng.* **2019**, *4*, 379−385.

(10) Zhang, H.; Zhang, X.; Shiue, E.; Fedkiw, P. S. Single-Ion Conductors for Lithium Batteries via Silica Surface Modification. *J. Power Sources* **2008**, *177*, 561−565.

(11) Merrill, L. C.; Chen, X. C.; Zhang, Y.; Ford, H. O.; Lou, K.; Zhang, Y.; Yang, G.; Wang, Y.; Wang, Y.; Schaefer, J. L.; Dudney, N. J. Polymer-Ceramic Composite Electrolytes for Lithium Batteries: A Comparison between the Single-Ion-Conducting Polymer Matrix and Its Counterpart. *ACS Appl. Energy Mater.* **2020**, *3*, 8871−8881.

(12) Long, L.; Wang, S.; Xiao, M.; Meng, Y. Polymer Electrolytes for Lithium Polymer Batteries. *J. Mater. Chem. A* **2016**, *4*, 10038−10069.

(13) Zhao, S.; Song, S.; Wang, Y.; Keum, J.; Zhu, J.; He, Y.; Sokolov, A. P.; Cao, P. F. Unraveling the Role of Neutral Units for Single-Ion Conducting Polymer Electrolytes. *ACS Appl. Mater. Interfaces* **2021**, *13*, 51525−51534.

(14) Zhu, J.; Zhang, Z.; Zhao, S.; Westover, A. S.; Belharouak, I.; Cao, P. F. Single-Ion Conducting Polymer Electrolytes for Solid-State Lithium−Metal Batteries: Design, Performance, and Challenges. *Adv. Energy Mater.* **2021**, *11*, 1−18.

(15) Cao, P. F.; Li, B.; Yang, G.; Zhao, S.; Townsend, J.; Xing, K.; Qiang, Z.; Vogiatzis, K. D.; Sokolov, A. P.; Nanda, J.; Saito, T. Elastic Single-Ion Conducting Polymer Electrolytes: Toward a Versatile

Approach for Intrinsically Stretchable Functional Polymers. *Macromolecules* **2020**, *53*, 3591−3601.
(16) Borzutzki, K.; Dong, D.; Wölke, C.; Kruteva, M.; Stellhorn, A.; Winter, M.; Bedrov, D.; Brunklaus, G. Small Groups, Big Impact: Eliminating Li+ Traps in Single-Ion Conducting Polymer Electrolytes. *iScience* **2020**, *23*, No. 101417.
(17) Zhang, W.; Feng, S.; Huang, M.; Qiao, B.; Shigenobu, K.; Giordano, L.; Lopez, J.; Tatara, R.; Ueno, K.; Dokko, K.; Watanabe, M.; Shao-Horn, Y.; Johnson, J. A. Molecularly Tunable Polyanions for Single-Ion Conductors and Poly(Solvate Ionic Liquids). *Chem. Mater.* **2021**, *33*, 524−534.
(18) Borzutzki, K.; Thienenkamp, J.; Diehl, M.; Winter, M.; Brunklaus, G. Fluorinated Polysulfonamide Based Single Ion Conducting Room Temperature Applicable Gel-Type Polymer Electrolytes for Lithium Ion Batteries. *J. Mater. Chem. A* **2019**, *7*, 188−201.
(19) Ford, H. O.; Park, B.; Jiang, J.; Seidler, M. E.; Schaefer, J. L. Enhanced Li+ Conduction within Single-Ion Conducting Polymer Gel Electrolytes via Reduced Cation−Polymer Interaction. *ACS Mater. Lett.* **2020**, *2*, 272−279.
(20) Boz, B.; Dev, T.; Salvadori, A.; Schaefer, J. L. Review—Electrolyte and Electrode Designs for Enhanced Ion Transport Properties to Enable High Performance Lithium Batteries. *J. Electrochem. Soc.* **2021**, *168*, No. 090501.
(21) Nguyen, H. D.; Kim, G. T.; Shi, J.; Paillard, E.; Judeinstein, P.; Lyonnard, S.; Bresser, D.; Iojoiu, C. Nanostructured Multi-Block Copolymer Single-Ion Conductors for Safer High-Performance Lithium Batteries. *Energ. Environ. Sci.* **2018**, *11*, 3298−3309.
(22) Oh, H.; Xu, K.; Yoo, H. D.; Kim, D. S.; Chanthad, C.; Yang, G.; Jin, J.; Ayhan, I. A.; Oh, S. M.; Wang, Q. Poly(Arylene Ether)-Based Single-Ion Conductors for Lithium-Ion Batteries. *Chem. Mater.* **2016**, *28*, 188−196.
(23) Yu, X.; Wang, L.; Ma, J.; Sun, X.; Zhou, X.; Cui, G. Selectively Wetted Rigid−Flexible Coupling Polymer Electrolyte Enabling Superior Stability and Compatibility of High-Voltage Lithium Metal Batteries. *Adv. Energy Mater.* **2020**, *10*, 1903939.
(24) Pandian, A. S.; Chen, X. C.; Chen, J.; Lokitz, B. S.; Ruther, R. E.; Yang, G.; Lou, K.; Nanda, J.; Delnick, F. M.; Dudney, N. J. Facile and Scalable Fabrication of Polymer-Ceramic Composite Electrolyte with High Ceramic Loadings. *J. Power Sources* **2018**, *390*, 153−164.
(25) Chen, L.; Huang, Y. F.; Ma, J.; Ling, H.; Kang, F.; He, Y. B. Progress and Perspective of All-Solid-State Lithium Batteries with High Performance at Room Temperature. *Energy Fuel* **2020**, *34*, 13456−13472.
(26) Judez, X.; Zhang, H.; Li, C.; Eshetu, G. G.; Zhang, Y.; González-Marcos, J. A.; Armand, M.; Rodriguez-Martinez, L. M. Polymer-Rich Composite Electrolytes for All-Solid-State Li-S Cells. *J. Phys. Chem. Lett.* **2017**, *8*, 3473−3477.
(27) Li, S.; Zhang, S. Q.; Shen, L.; Liu, Q.; Ma, J. B.; Lv, W.; He, Y. B.; Yang, Q. H. Progress and Perspective of Ceramic/Polymer Composite Solid Electrolytes for Lithium Batteries. *Adv. Sci.* **2020**, *7*, No. 1903088.
(28) Zhou, Q.; Ma, J.; Dong, S.; Li, X.; Cui, G. Intermolecular Chemistry in Solid Polymer Electrolytes for High-Energy-Density Lithium Batteries. *Adv. Mater.* **2019**, *31*, 1902029.
(29) Croce, F.; Persi, L. L.; Scrosati, B.; Serraino-Fiory, F.; Plichta, E.; Hendrickson, M. A. Role of the Ceramic Fillers in Enhancing the Transport Properties of Composite Polymer Electrolytes. *Electrochim. Acta* **2001**, *46*, 2457−2461.
(30) Srivastava, S.; Schaefer, J. L.; Yang, Z.; Tu, Z.; Archer, L. A. 25th Anniversary Article: Polymer-Particle Composites: Phase Stability and Applications in Electrochemical Energy Storage. *Adv. Mater.* **2014**, *26*, 201−234.
(31) Elmore, C. T.; Seidler, M. E.; Ford, H. O.; Merrill, L. C.; Upadhyay, S. P.; Schneider, W. F.; Schaefer, J. L. Ion Transport in Solvent-Free, Crosslinked, Single-Ion Conducting Polymer Electrolytes for Post-Lithium Ion Batteries. *Batteries* **2018**, *4*, 28.
(32) Bhattacharyya, A. J. Ion Transport in Liquid Salt Solutions with Oxide Dispersions: "Soggy Sand" Electrolytes. *J. Phys. Chem. Lett.* **2012**, *3*, 744−750.
(33) Pfaffenhuber, C.; Göbel, M.; Popovic, J.; Maier, J. Soggy-Sand Electrolytes: Status and Perspectives. *Phys. Chem. Chem. Phys.* **2013**, *15*, 18318−18335.
(34) Ma, Q.; Zhang, H.; Zhou, C.; Zheng, L.; Cheng, P.; Nie, J.; Feng, W.; Hu, Y. S.; Li, H.; Huang, X.; Chen, L.; Armand, M.; Zhou, Z. Single Lithium-Ion Conducting Polymer Electrolytes Based on a Super-Delocalized Polyanion. *Angew. Chem. Int. Ed.* **2016**, *55*, 2521−2525.
(35) Meziane, R.; Bonnet, J. P.; Courty, M.; Djellab, K.; Armand, M. Single-Ion Polymer Electrolytes Based on a Delocalized Polyanion for Lithium Batteries. *Electrochim. Acta* **2011**, *57*, 14−19.
(36) Chen, X. C.; Zhang, Y.; Merrill, L. C.; Soulen, C.; Lehmann, M. L.; Schaefer, J. L.; Du, Z.; Saito, T.; Dudney, N. J. Gel Composite Electrolyte - an Effective Way to Utilize Ceramic Fillers in Lithium Batteries. *J. Mater. Chem. A* **2021**, *9*, 6555−6566.
(37) McGuinness, S. R.; Wilkinson, J. T.; Tighe, M. E.; Majumdar, A.; Mulder, B.; Stech, E.; Robertson, D.; Peaslee, G. F. Development of the St. Andre Ion Beam Analysis Facility at Notre Dame. *AIP Conf. Proc.* **2019**, *2160*, No. 050025.
(38) Wilkinson, J. T.; McGuinness, S. R.; Peaslee, G. F. External Beam Normalization Measurements Using Atmospheric Argon Gamma Rays. *Nucl. Instruments Methods Phys. Res. Sect. B Beam Interact. with Mater. Atoms* **2020**, *484*, 1−4.
(39) Mark, J. E. *Polymer Data Handbook*; 2nd Ed., Journal of the American Chemical Society, 2009; *131*, 425−850.
(40) Propylene Carbonate Solvent Properties https://macro.lsu.edu/howto/solvents/Propylene%20Carbonate.htm.
(41) Wohlfarth, C. Static Dielectric Constant of Tetraethylene Glycol Dimethyl Ether. *In Static Dielectric Constants of Pure Liquids and Binary Liquid Mixtures*; Springer Berlin Heidelberg, 2015, 201−201.
(42) Herstedt, M.; Smirnov, M.; Johansson, P.; Chami, M.; Grondin, J.; Servant, L.; Lassègues, J. C. Spectroscopic Characterization of the Conformational States of the Bis(Trifluoromethanesulfonyl)Imide Anion (TFSI-). *J. Raman Spectrosc.* **2005**, *36*, 762−770.
(43) Rey, I.; Lassègues, J. C.; Grondin, J.; Servant, L. Infrared and Raman Study of the PEO-LiTFSI Polymer Electrolyte. *Electrochim. Acta* **1998**, *43*, 1505−1510.
(44) Hardwick, L. J.; Holzapfel, M.; Wokaun, A.; Novák, P. Raman Study of Lithium Coordination in EMI-TFSI Additive Systems as Lithium-Ion Battery Ionic Liquid Electrolytes. *J. Raman Spectrosc.* **2007**, *38*, 110−112.
(45) Lassègues, J. C.; Grondin, J.; Aupetit, C.; Johansson, P. Spectroscopic Identification of the Lithium Ion Transporting Species in LiTFSI-Doped Ionic Liquids. *J. Phys. Chem. A* **2009**, *113*, 305−314.
(46) Tchitchekova, D. S.; Monti, D.; Johansson, P.; Bardé, F.; Randon-Vitanova, A.; Palacín, M. R.; Ponrouch, A. On the Reliability of Half-Cell Tests for Monovalent (Li+, Na+) and Divalent (Mg2+, Ca2+) Cation Based Batteries. *J. Electrochem. Soc.* **2017**, *164*, A1384−A1392.
(47) Fujii, K.; Fujimori, T.; Takamuku, T.; Kanzaki, R.; Umebayashi, Y.; Ishiguro, S. I. Conformational Equilibrium of Bis-(Trifluoromethanesulfonyl) Imide Anion of a Room-Temperature Ionic Liquid: Raman Spectroscopic Study and DFT Calculations. *J. Phys. Chem. B* **2006**, *110*, 8179−8183.
(48) Henderson, W. A.; Seo, D. M.; Han, S.-D.; Borodin, O. Electrolyte Solvation and Ionic Association. VII. Correlating Raman Spectroscopic Data with Solvate Species. *J. Electrochem. Soc.* **2020**, *167*, 110551.
(49) Ford, H. O.; Merrill, L. C.; He, P.; Upadhyay, S. P.; Schaefer, J. L. Cross-Linked Ionomer Gel Separators for Polysulfide Shuttle Mitigation in Magnesium−Sulfur Batteries: Elucidation of Structure−Property Relationships. *Macromolecules* **2018**, *51*, 8629−8636.
(50) Gebel, G.; Diat, O. Neutron and X-Ray Scattering: Suitable Tools for Studying Lonomer Membranes. *Fuel Cells* **2005**, *5*, 261−276.

https://doi.org/10.1021/acsapm.1c01535
ACS Appl. Polym. Mater. 2022, 4, 1095−1109

(51) Ford, H. O.; Cui, C.; Schaefer, J. L. Comparison of Single-Ion Conducting Polymer Gel Electrolytes for Sodium, Potassium, and Calcium Batteries: Influence of Polymer Chemistry, Cation Identity, Charge Density, and Solvent on Conductivity. *Batteries* **2020**, *6*, 11.
(52) Wang, J. H. H.; Yang, C. H. C.; Masser, H.; Shiau, H. S.; O'Reilly, M. V.; Winey, K. I.; Runt, J.; Painter, P. C.; Colby, R. H. Ion States and Transport in Styrenesulfonate Methacrylic PEO9 Random Copolymer Ionomers. *Macromolecules* **2015**, *48*, 7273−7285.
(53) Chen, X. C.; Liu, X.; Samuthira Pandian, A.; Lou, K.; Delnick, F. M.; Dudney, N. J. Determining and Minimizing Resistance for Ion Transport at the Polymer/Ceramic Electrolyte Interface. *ACS Energy Lett.* **2019**, *4*, 1080−1085.
(54) Chen, C.; Jiang, M.; Zhou, T.; Raijmakers, L.; Vezhlev, E.; Wu, B.; Schülli, T. U.; Danilov, D. L.; Wei, Y.; Eichel, R. A.; Notten, P. H. L. Interface Aspects in All-Solid-State Li-Based Batteries Reviewed. *Adv. Energy Mater.* **2021**, *11*, No. 2003939.
(55) Mateus, R.; Jesus, A. P.; Braizinha, B.; Cruz, J.; Pinto, J. V.; Ribeiro, J. P. Proton-Induced γ-Ray Analysis of Lithium in Thick Samples. *Nucl. Instruments Methods Phys. Res. Sect. B Beam Interact. with Mater. Atoms* **2002**, *190*, 117−121.
(56) Demortier, G. Analysis of Light Elements with a Nuclear Microprobe - A Review. *Nucl. Instrum. Methods Phys. Res., Sect. B* **1995**, *104*, 244−254.
(57) Wolfenstine, J. Stability Predictions of Solid Li-Ion Conducting Membranes in Aqueous Solutions. *J. Mater. Sci.* **2010**, *45*, 3954−3956.

https://doi.org/10.1021/acsapm.1c01535
ACS Appl. Polym. Mater. 2022, 4, 1095−1109